where

$$kT_k' = \exp\left[-\frac{8\pi}{\Gamma}\left(\frac{\bar{E}^2-\frac{3}{4}J^2}{\bar{E}-\frac{11}{2}J}\right)-8\left(\frac{J+\frac{3}{2}\bar{E}}{\bar{E}-\frac{11}{2}J}\right)\ln U + \left(\frac{13\bar{E}+\frac{5}{2}J}{\bar{E}-\frac{11}{2}J}\right)\ln 2J\right], \quad (6.26)$$

$$\bar{E} = E + \mathrm{Re}\Lambda_1.$$

Values of ω satisfying (6.25) give the approximate location of the anomalous resonances. We find that in terms of the new Kondo temperature, T_K', (6.25) is identical to (2.14). Hence, in contrast to the results found in Sec. V for the diagonal exchange coupling where the anomalous resonances are driven away from the Fermi surface, here we find that for $J>\frac{2}{3}\sqrt{3}|E|$ the anomalous resonances are returned to the region of the Fermi surface. In the large J limit, (6.26) may be written approximately as

$$kT_K' \cong U\left(\frac{U}{2J}\right)^{5/11}\exp\left(-\frac{12}{11}\right)\left(\frac{\pi J}{\Gamma}\right), \quad \text{(large } U, J \text{ limit)}. \quad (6.27)$$

The exponents 5/11 and 12/11 have no ready explanation, but otherwise this result is not qualitatively different from the one-orbital model. We have thus shown that despite the vast complications which degeneracy introduces into the mathematics, the physical results did not change drastically in the appropriate limit.

PHYSICAL REVIEW VOLUME 178, NUMBER 2 10 FEBRUARY 1969

Ultrasonic Propagation in $RbMnF_3$. I. Elastic Properties*

R. L. MELCHER†
Arthur H. Compton Laboratory of Physics, Washington University, St. Louis, Missouri 63130
and
Laboratory of Atomic and Solid State Physics, Cornell University, Ithaca, New York 14850

AND

D. I. BOLEF
Arthur H. Compton Laboratory of Physics, Washintgon University, St. Louis, Missouri 63130

(Received 14 October 1968)

The elastic properties of $RbMnF_3$ have been investigated over the temperature range 4.2–300°K with a continuous-wave transmission technique. The measured values of the three adiabatic elastic constants C_{11}, C_{44}, and $C'=\frac{1}{2}(C_{11}-C_{12})$ at 300°K in units of 10^{12} erg/cm^3 are, respectively, 1.174±0.002, 0.3193±0.0008, and 0.3763±0.0008. The value of the Debye temperature calculated from the low-temperature elastic-constant data is Θ_D(elastic)=386±1.5°K. For $T>\frac{1}{2}\Theta_D$, the three elastic constants decrease linearly with temperature. Attempts at applying the present results to a three-force-constant theory of the cubic perovskite structure failed because the secular determinant for the principal oscillation frequencies results in an unstable solution. It is found that only the longitudinal elastic modes are affected by the onset of long-range order at the Néel temperature T_N. This is consistent with Pytte and Bennett's recent theory if the dominant spin-phonon interaction is taken to be the volume magnetostriction. In the antiferromagnetic state, the elastic constants are found to be sharply dependent on applied magnetic fields. A model is proposed which explains the magnetic-field dependence and temperature dependence of the elastic constants in this region. The basis of the model is that the coupling of the ultrasonic waves to the antiferromagnetic resonance modes in the low-frequency limit is determined by the sublattice magnetization orientation, which in turn is magnetic-field-dependent. This model will be described in more detail in a second paper.

I. INTRODUCTION

THE elastic and magnetoelastic properties of materials which undergo antiferromagnetic ordering transitions have been of considerable interest in recent years. In sinlge-crystal specimens, interest has focused primarily on the temperature dependence of the elastic constants and/or the ultrasonic attenuation at or near the antiferromagnetic ordering tempera-

* Research sponsored in part by the National Science Foundation under Grant No. GP-7931 and the U. S. Air Force Office of Scientific Research under Grant No. 68-1412 PR.

† Present address: Laboratory of Atomic and Solid State Physics, Cornell University, Ithaca, N. Y.

ture.[1–12] More recently the changes in the elastic constants and ultrasonic attenuation on application of magnetic fields large enough to cause significant reorientation of the magnetic sublattices in the ordered state have been studied. Shapira[13] and Shapira and Zak[14] have demonstrated several interesting effects in the ultrasonic attenuation for applied fields at or near the "spin-flop" region in the uniaxial antiferromagnet MnF_2. Similar effects on both the ultrasonic attenuation and velocity were observed by Melcher *et al.* in the cubic antiferromagnet $RbMnF_3$.[8]

In this paper we present an experimental study of the elastic properties of $RbMnF_3$ over the temperature range 4.2–300°K and in magnetic fields of zero and 7.5 kOe. The adiabatic elastic constants C_{11}, C_{44}, $C'=\frac{1}{2}(C_{11}-C_{12})$, and $C_L=\frac{1}{2}(C_{11}+C_{12}+2C_{44})$ have been calculated from the measured phase velocity of both longitudinal and transverse 30-MHz ultrasonic waves propagating along the [100] or [110] axes of this cubic material. The bulk modulus, the anisotropy ratio, and the elastic Debye temperature have been calculated from the measured values of the elastic constants. A model is outlined which explains the magnetic-field dependence of the elastic constants in the antiferromagnetic state of $RbMnF_3$.

In a second paper (to be referred to as II) we shall present a theoretical and experimental study of the effect of applied magnetic fields on the elastic properties $RbMnF_3$ in the ordered state. The model outlined in Sec. IV of this paper will be described in detail in II and a quantitative comparison to several experimental cases will be made. A third paper (III) will be devoted to a study of the coupling between the ultrasonic waves and the fluorine nuclear spin system in $RbMnF_3$ (i.e., nuclear acoustic resonance).[15,16]

$RbMnF_3$ crystallizes in the ideal cubic perovskite structure belonging to the $O_h(m3m)$ point group and has five atoms per unit cell. The length of the unit cell at room temperature is 4.234 ± 0.001 Å,[17] and the theoretical room-temperature density is 4.317 ± 0.004 g/cm^3. Its cubic symmetry is believed to be maintained at all temperatures[18] and the peak in the thermal expansion at Néel temperature ($T_N=83$°K) is anomalously small when compared to that of other antiferromagnets, thus indicating a very stable lattice structure.[19]

Many of the perovskite oxides (e.g., $BaTiO_3$, $SrTiO_3$, etc.) are known to undergo ferro- or antiferro-electric phase transitions which are accompanied by distortion of the lattice to a lower crystallographic symmetry.[20] Many of the alkali—transition-metal—fluorides (e.g., $KMnF_3$, NH_4MnF_3, $RbFeF_3$, $KCoF_3$, etc.) undergo similar phase transitions which are apparently not associated with ferroelectric ordering.[9,21,22] The distortion of these fluoride compounds is often, but not always (e.g., $KMnF_3$[21] has a purely crystallographic phase transition at $T\simeq180$°K and undergoes further distortion at its magnetic ordering temperature $T_N\simeq88$°K), associated with antiferromagnetic ordering. Associated with the stability of the $RbMnF_3$ lattice is a Goldschmit tolerance ratio of 1.00, whereas for $NaMnF_3$, $KMnF_3$, NH_4MnF_3, and $CsMnF_3$ the respective ratios are 0.81, 0.94, 0.97, and 1.05.[17] Since the crystallographic phase transitions produce marked anomalies in the elastic properties of these materials,[4,5,9,23] it is of considerable interest to carry out a systematic study of the elastic properties of an ideal perovskite, i.e., $RbMnF_3$ which remains cubic at all temperatures. The room-temperature elastic constants have been measured perviously by Eastman.[24]

In addition to its attractive structural properties, the low magnetic anistropy[18] ($H_A\simeq4$ Oe) of $RbMnF_3$ (a result of the combination of cubic symmetry and of the Mn^{++} ion having the $3d^5$ configuration and ^6S ground state) has made possible several detailed studies of the antiferromagnetic resonance properties of $RbMnF_3$ in the conventional microwave bands (e.g., X and K).[24–26] The low magnetic anisotropy has resulted also in interesting experiments on the coupling of the antiferromagnetic magnon modes to the Mn^{55} nuclear spin system.[27] Neutron-diffraction work indicates that the magnetic properties of $RbMnF_3$ are well described by a two-sublattice molecular-field model

[1] J. R. Neighbours, R. W. Oliver, and C. H. Stillwell, Phys. Rev. Letters **11**, 125 (1963).
[2] D. I. Bolef and J. de Klerk, Phys. Rev. **129**, 1063 (1963).
[3] E. J. O'Brien and J. Franklin, J. Appl. Phys. **37**, 2809 (1966).
[4] K. S. Aleksandrov, L. M. Reshchikova, and B. U. Beznosikov, Phys. Status Solidi **18**, K17 (1966).
[5] K. S. Aleksandrov, L. M. Reshchikova, and B. U. Beznosikov, Fiz. Tverd. Tela **8**, 3637 (1966) [English transl.: Soviet Phys.—Solid State **8**, 2904 (1967)].
[6] O. G. Brandt and C. T. Walker, Phys. Rev. Letters **18**, 11 (1967).
[7] K. Walther, Solid State Commun. **5**, 399 (1967).
[8] R. L. Melcher, D. I. Bolef, and R. W. H. Stevenson, Solid State Commun. **5**, 735 (1967).
[9] L. R. Testardi, H. J. Levinstein, and H. J. Guggenheim, Phys. Rev. Letters **19**, 503 (1967).
[10] B. Golding, Phys. Rev. Letters **20**, 5 (1968).
[11] M. Rosen, Phys. Rev. **165**, 357 (1968).
[12] O. G. Brandt and C. T. Walker, Phys. Rev. **170**, 528 (1968).
[13] Y. Shapira, Phys. Letters **24A**, 361 (1967).
[14] Y. Shapira and J. Zak, Phys. Rev. **170**, 503 (1968).
[15] R. L. Melcher, D. I. Bolef, and R. W. H. Stevenson, Phys. Rev. Letters **20**, 453 (1968).
[16] R. L. Melcher and D. I. Bolef, Phys. Rev. Letters **20**, 1338 (1968).
[17] Yu P. Siamanov, L. P. Batsanova, and L. M. Kouba, Zh. Neorgan. Khim. **2**, 2410 (1957).
[18] D. T. Teaney, M. J. Freiser, and R. W. H. Stevenson, Phys. Rev. Letters **9**, 212 (1962).
[19] D. T. Teaney, V. L. Moruzzi, and B. E. Argyle, J. Appl. Phys. **37**, 1122 (1966).
[20] F. P. Jona and G. Shirane, *Ferroelectric Crystals* (Pergamon Press, Inc., New York, 1962), Chap. V.
[21] O. Beckman and K. Knox, Phys. Rev. **121**, 376 (1961).
[22] J. D. Axe and G. D. Pettit, Phys. Rev. **157**, 435 (1967).
[23] R. O. Bell and G. Rupprecht, Phys. Rev. **129**, 90 (1963).
[24] D. E. Eastman, Phys. Rev. **156**, 645 (1967).
[25] M. J. Freiser, R. J. Joenk, P. E. Seiden, and D. T. Teaney, in *Proceedings of the International Conference on Magnetism, Nottingham, 1964* (The Institute of Phys. and the Physical Society, London, 1965), p. 432.
[26] P. H. Cole and W. J. Ince, Phys. Rev. **150**, 377 (1966).
[27] A. J. Heeger and D. T. Teaney, J. Appl. Phys. **35**, 846 (1964).

in which the easy axes are the four equivalent [111] directions.[28]

An additional result of the low magnetic anisotropy is the dependence of the equilibrium sublattice magnetization orientation on applied magnetic fields of magnitudes available from conventional laboratory magnets [the reorientation field, $H_c \sim (2H_E H_A)^{1/2}$, is of the order of 2.5 kOe in $RbMnF_3$].[26] As will be discussed briefly in Sec. IV and more completely in II this reorientation results in rather large effects on the elastic properties of the medium.[8,29]

In Sec. II the samples, their preparation, and the experimental techniques used to measure the ultrasonic velocity are described. The experimental results are presented in Sec. III. Discussion of the three main temperature regions of interest, i.e., paramagnetic, critical, and the antiferromagnetic regions, is given in Sec. IV. Finally, in Sec. V, a summary of the conclusions drawn from this study is given.

II. EXPERIMENTAL

A. Samples and Their Preparation

Two single-crystal specimens of $RbMnF_3$ (designated *S3A* and *S3B*), both cut from the same boule, were used in the present study. The ultrasonic propagation direction in *S3A* was the [100] axis and in *S3B* the [110] axis; the respective path lengths were 0.7950 and 0.8235 cm. The approximately rectangular cross sections of the samples were large enough to accommodate $\frac{1}{4}$-in. quartz transducers. The crystals were optically clear (pink in color) with the exception of a few very small bubbles visible only after polishing and under a microscope. Chemical analysis of pieces from the same boule yielded 10–100 ppm of silicon and 1–10 ppm each of the following metallic elements: Mg, Cr, Fe, Al, Ca, Na, and K. The crystals were oriented to within $\pm 1°$ by Laue back-reflection x-ray photographs. After cutting specimens of the desired size and orientation from the original boule with a diamond-impregnated cutting wheel, opposite surfaces of the samples were ground flat ($<2\times10^{-5}$ cm) and parallel ($<5\times10^{-5}$ cm) with Al_2O_3 (9.0, 5.0, 3.0, 1.0, and 0.3 μ grit) on cast iron and lead laps.

B. Cryogenics

The sample was mounted in a large copper holder, the temperature of which was maintained constant to within $\pm 0.1°K$ for each measurement by means of a servoregulated temperature controller (Artronix Model 6601). In the neighborhood of the critical region the temperature was maintained to $\pm 0.01°K$ stability. The absolute accuracy of the temperature measurements made with platinum (Rosemount #118MC) and germanium (Cryocal #S/N285) resistance thermometers was $\pm 0.5°K$ and the relative accuracy $\pm 0.1°K$. No thermal gradients greater than $0.005°K$ were detected between sensors and sample.

C. Velocity Measurements

A transmission-type continuous-wave technique similar to that described by Melcher *et al.*[30] was used to measure the ultrasonic phase velocity. This technique involves the accurate measurement of the frequency of the nth mechanical resonance, i.e., the nth harmonic of elastic vibration of the composite resonator consisting of the sample and the two (transmitting and receiving) quartz transducers. This angular frequency ω_n can then be related to the ultrasonic phase velocity v in the sample:

$$v=\frac{l_s\omega_n}{n\pi}\left[1-2\frac{\rho_T l_T}{\rho_s l_s}\left(\frac{\omega_T-\omega_n}{\omega_n}\right)\right], \tag{1}$$

where the number n of the harmonic involved is given by

$$n=\frac{\omega_n}{\Delta}\left(1-2\frac{\rho_T l_T}{\rho_s l_s}\right). \tag{2}$$

The length and density, respectively, of the sample are l_s and ρ_s and of the transducers are l_T and ρ_T. ω_T is the resonant angular frequency of the transducer and Δ is the angular frequency between the nth and $(n+1)$th mechanical resonances. The factor of 2 in the mass correction terms of Eqs. (1) and (2) is a consequence of the transmission system in which two transducers are used. Conditions under which the above equations are valid are discussed by Bolef and Menes[31] and by Bolef and de Klerk[32] for the equivalent reflection (single transducer) system.

Under ideal circumstances the shape of a mechanical resonance closely approximates a Lorentzian curve, its quality factor being easily related to the acoustic losses in the sample. Careless sample preparation, misorientation of the crystallographic axes, or poor transducer-sample bonds often results in "structure" on the mechanical resonances. Physical processes in the sample can produce similar effects. Magnetoelastic coupling in magnetic materials causes, in the weak-coupling limit, a relatively small shift in the frequency of a mechanical resonance (i.e., in the phase velocity) and no significant effect on the mechanical resonance shape. In the case of stronger coupling, however, the resonance modes of the sample are no longer describable as elastic or magnetic but must be considered to be magnetoelastic modes. This can cause severe distortion of the

[28] S. J. Pickart, H. A. Alperin, and R. Nathans, J. Phys. (Paris) **25**, 565 (1964).
[29] R. L. Melcher, Ph.D. thesis, Washington University, 1968 (unpublished).
[30] R. L. Melcher, D. I. Bolef, and J. B. Merry, Rev. Sci. Instr. **39**, 1618 (1968).
[31] D. I. Bolef and M. Menes, J. Appl. Phys. **31**, 1010 (1960).
[32] D. I. Bolef and J. de Klerk, IEEE Trans. Ultrasonics Eng. **10**, 19 (1963).

mechanical resonance pattern (and, equivalently, non-exponential echo decay when using pulse techniques). The purely elastic stress wave (which in the absence of magnetolastic effects is not coupled to other modes, elastic or magnetic) generated at one surface of the sample is now coupled to other essentially elastic, as well as to magnetic, modes through the magnetoelastic interaction. The disortion of the mechanical resonances is accompanied by increased attenuation if additional loss mechanisms exist (i.e., magnon damping).

Shown in Fig. 1 are three continuous-wave (cw) mechanical response patterns in $RbMnF_3$. In Figs. 1(a) and 1(b) longitudinal waves were propagated along the [110] axis at $T=77.4$ and 54.6°K, respectively. In Fig. 1(c) transverse waves were propgated along [110] with $\hat{e}\|[1\bar{1}0]$ at 77.4°K. Figure 1(a) demonstrates weak magnetoelastic coupling (no distortion of the pattern); Fig. 1(b) demonstrates strong coupling (splitting of the individual mechanical resonances into two or more peaks); Fig. 1(c) shows very strong coupling resulting in almost complete destruction of the mechanical resonance pattern making elastic velocity measurements almost meaningless. The receiver gain in Fig. 1(c) has been increased by 28 dB over that in Figs. 1(a) and 1(b).

The measurements reported in the following section were all made at 30 MHz using the "dc" cw technique as described in Ref. 30. X- and AT-cut resonant quartz transducers were used to generate longitudinal and transverse waves, respectively. Either silicone grease or Non-aq stopcock grease were used as transducer specimen bonds. The absolute accuracy in the values of the elastic constants is $\pm 0.2\%$ and the relative accuracy is $\pm 0.004\%$. In the temperature region near 60°K the errors are considerably larger due to the strong magnetoelastic coupling resulting in the effects discussed above. The data of Ref. 19 were used to correct for thermal expansion.

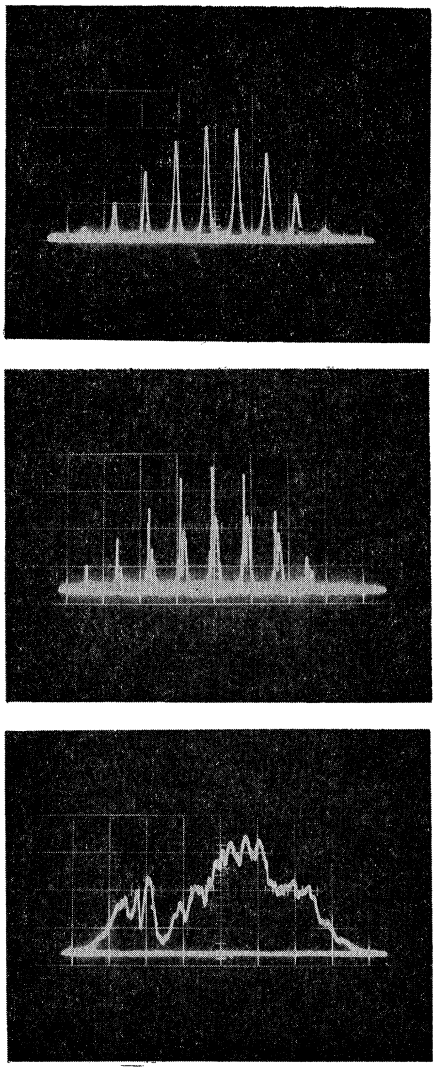

FIG. 1. Mechanical response patterns for 30 MHz ultrasonic waves in $RbMnF_3$ No. $S3B$, $H_0=0$. (a) longitudinal waves, $\mathbf{k}\|[110]$, $T=77.4$°K; (b) longitudinal waves, $\mathbf{k}\|[110]$, $T=54.6$°K; and (c) transverse waves, $\mathbf{k}\|[110]$, $\hat{e}\|[1\bar{1}0]$, $T=77.4$°K. Receiver gain increased in (c) by 28 dB over that in (a) and (b).

III. EXPERIMENTAL RESULTS

The measured values of the adiabatic elastic constants of $RbMnF_3$ over the temperature range 4.2–300°K are shown in Figs. 2–5. Also shown in these figures are the effects on the elastic constants of applying magnetic fields of magnitude 7.5 kOe and with the indicated orientations. Consistency checks for the three independent elastic constants obtained from these four sets of data indicate agreement well within the quoted absolute error of $\pm 0.2\%$ for temperatures $T>T_N$. For $T<T_N$ magnetoelastic effects lower the effective elastic symmetry and consistency (assuming cubic symmetry) is not expected. Measurements of C_{44} (not shown here) obtained from transverse propagation along [100] in sample $S3A$ agree both absolutely and relatively with the data of Fig. 4 to the stated accuracy, thus providing a further check. A final consistency check was made by measuring C_{11} in a third sample of $RbMnF_3$ cut from a different boule; the results (not shown here) agree with the data of Fig. 2.

No ambiguity in the data exists for $T>T_N$; however, for $T<T_N$ some explanation is necessary. In most cases the magnetic-field dependence of the elastic constants can be treated in the weak-coupling limit of the appropriate magnetoelastic theory as outlined in Sec. IV. However, in the region near 60°K the weak-coupling limit is found to be no longer valid,[33] considerable scatter exists in the data due to the structured

[33] For the case of C_{44} the weak-coupling limit is valid at all temperatures because the magnetoelastic coupling constant, which is a measure of the strength of the coupling to this mode, is a factor of 10 less (hence the effect is 10^2 weaker) than the coupling constants for each of the other modes (see Fig. 4). This result will be derived in II.

TABLE I. Elastic properties of $RbMnF_3$.

	4.2°K		300°K	
	$H_0=0$	$H_0=7.5$ kOe $\mathbf{H_0}\|\|\mathbf{k}$	Independent of H_0	Athermal
$C_{11}(10^{12}$ erg/cm$^3)$	1.266 ±0.002	1.275 ±0.002	1.174 ±0.002	1.307 ±0.004
Temp. coef. of C_{11} at 300°K (ppm/°K)			349±8	
$C_{44}(10^{12}$ erg/cm$^3)$	0.3281±0.0008	0.3281±0.0008	0.3193±0.0008	0.3278±0.001
Temp. coef. of C_{44} at 300°K (ppm/°K)			88.7 ±1.5	
$C'=\frac{1}{2}(C_{11}-C_{12})$ $(10^{12}$ erg/cm$^3)$	0.4253±0.0008	0.4266±0.0008	0.3763±0.0008	0.442 ±0.001
Temp. coef. of C' at 300°K (ppm/°K)			585±10	
$B=\frac{1}{3}(C_{11}+2C_{12})$ $(10^{12}$ erg/cm$^3)$	0.701 ±0.002	0.708 ±0.002	0.675 ±0.002	0.755 ±0.004
$A=2C_{44}/(C_{11}-C_{12})$	0.7715±0.002	0.7695±0.002	0.8490±0.002	0.741 ±0.004
Θ_D(elastic) (°K)	386.4 ±1.5	386.0 ±1.5	375.0 ±1.5	389.2 ±2.0
ρ_s(g/cm^3)	4.356 ±0.01		4.317 ±0.005	4.391 ±0.008[a]

[a] Athermal value of ρ_s was obtained by extrapolation of the linear high-temperature variation of the lattice constant to absolute zero. This gives the length of the unit cell to be a(athermal) $=4.209\pm0.004$ Å.

mechanical resonances, and in some cases [Figs. 1(c) and 3] it was impossible to make measurements, over a narrow temperature range about 60°K, because of the high attenuation and structure. In this strong-coupling region the meaning of ultrasonic velocity measurements is obscure due to the magnetoelastic nature of the resonant modes.

The temperature region 4.2–100°K is shown in more detail in Figs. 6 and 7. Perhaps Fig. 7 illustrates most clearly the experimental situation. At 4.2°K the mechanical resonances were essentially Lorentzian and showed no structure. On increasing the temperature to about 45°K structure began to develop in the form of a "subsidiary peak" on each mechanical resonance. On further increasing the temperature the subsidiary peak increased in magnitude, the original peak decreasing

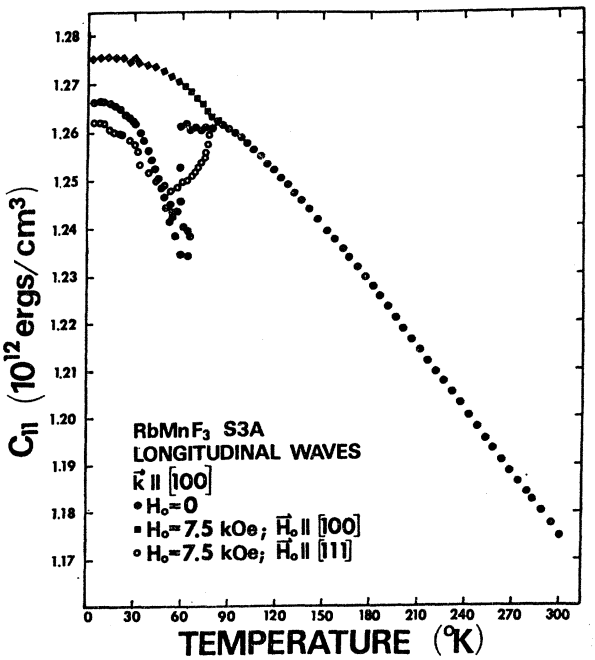

FIG. 2. Elastic constant C_{11} versus temperature in $RbMnF_3$.

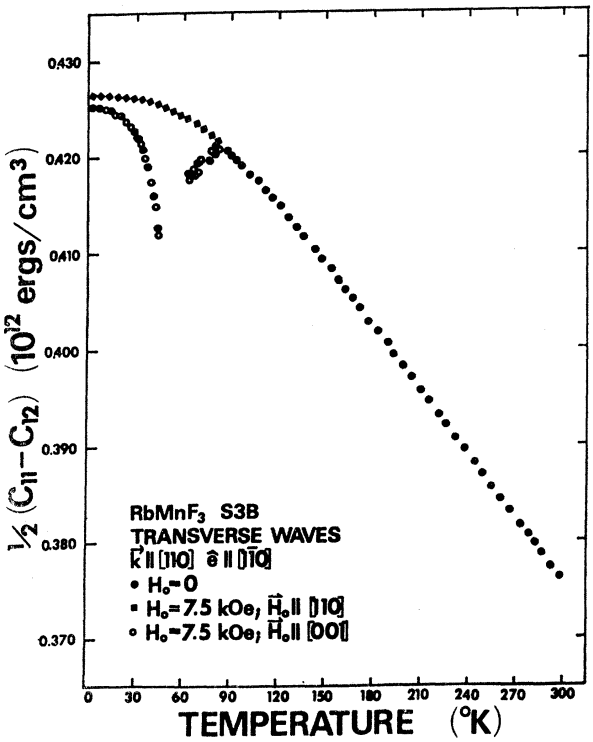

FIG. 3. Elastic constant $C'=\frac{1}{2}(C_{11}-C_{12})$ versus temperature in $RbMnF_3$.

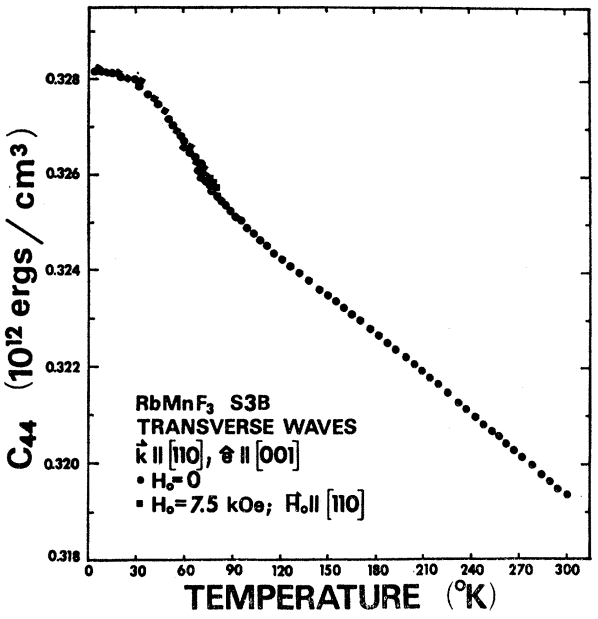

FIG. 4. Elastic constant C_{44} versus temperature in $RbMnF_3$.

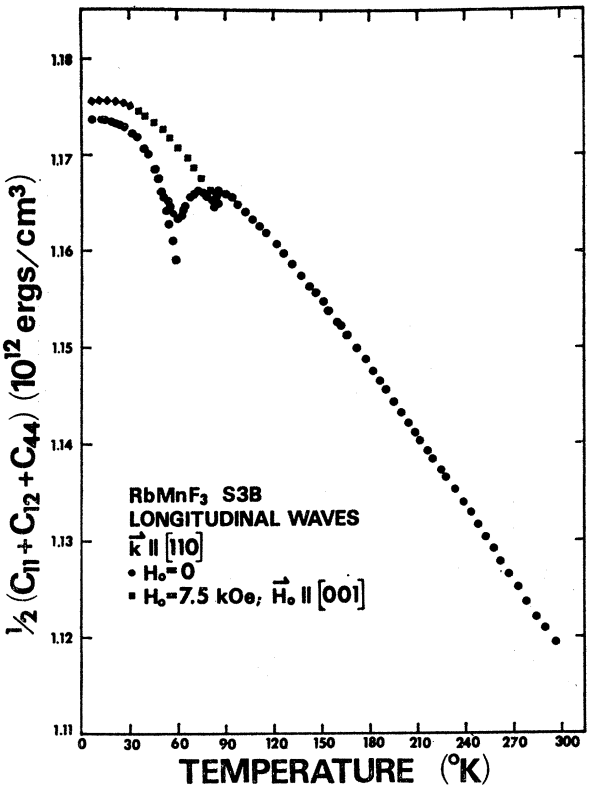

FIG. 5. Elastic constant $C_L=\frac{1}{2}(C_{11}+C_{12}+2C_{44})$ versus temperature in $RbMnF_3$.

until at $T\simeq 60$°K only the subsidiary peak could be observed. This peak then fitted smoothly to the high-temperature data. The elastic constant C_L, calculated using both peaks over the temperature range 45–60°K, is shown in Fig. 7. This behavior was reproducible from run to run, showed no hysteresis, was independent of whether the temperature was being increased or decreased during a given run, and could always be removed by application of a 7.5-kOe magnetic field in the appropriate direction.

For each elastic mode there is at least one orientation of the applied field for which the strong magnetoelastic effects at 60°K are absent, and for which the transition from the paramagnetic to antiferromagnetic state is smooth (with the exception, in some cases, of some effects of critical scattering at and near T_N, to be discussed in Sec. IV). At this orientation of $\mathbf{H}_0$, the elastic behavior is that expected of diamagnetic media. The data represented by the solid squares (except for Fig. 6, in which case these data are represented by triangles) will be referred to as the "pure" elastic constants and the remaining data points will be referred to as the "effective" elastic constants as modified by inclusion of magnetoelastic coupling, This notation will be justified in Sec. IV. There is no amibiguity in the pure-elastic-constant behavior at any temperature.

The Debye temperature as calculated from the elastic constants is plotted in Fig. 8 as a function of temperature. The value of Θ_D(elastic) was obtained from the relation

$$\Theta_D(\text{elastic})=\frac{h}{k}\left(\frac{3N}{4\pi V}\right)^{1/3}\left(\frac{C_{11}}{\rho_s}\right)^{1/2}g, \qquad (3)$$

where h is Planck's constant, k is Boltzmann's constant, N/V is the number density of atoms, and g is a number obtained by interpolation from graphs due originally to P. M. Marcus and reproduced in a review article by Alers.[34] The absolute accuracy of this determination of the Debye temperature is of the order of $\pm 0.5\%$; the relative accuracy is somewhat better. Thus no significance can be attached to the difference in Θ_D(elastic) at $T=4.2$°K for $H_0=0$ and $H_0=7.5$ kOe. However, the relative difference in their behavior with temperature is significant.

A summary of the elastic properties of $RbMnF_3$ at $T=4.2$°K and $T=300$°K is given in Table I. Included in the table are the so-called "athermal" values of the elastic constants. These are obtained by extrapolation of the linear high-temperature curve to absolute zero. It is these values of the elastic constants which are to be compared to a theory of the interatomic forces in the static, harmonic approximation, i.e., this extrapolation procedure eliminates anharmonic effects.[35] Also listed in Table I are the values of the bulk modulus $B=\frac{1}{3}(C_{11}+2C_{12})$, the density ρ_s, and the value of the temperature coefficient at 300°K of $C_{ij}(T)$,

$$-(\partial/\partial T)[\ln C_{ij}].$$

[34] G. A. Alers, *Physical Acoustics*, edited by W. P. Mason (Academic Press Inc., New York, 1965), Vol. III B.

[35] For a complete discussion of anharmonic effects in crystal lattice, see G. Leibfried and W. Ludwig, in *Solid State Physics*, edited by F. Seitz and D. Turnbull (Academic Press Inc., New York, 1961), Vol. 12.

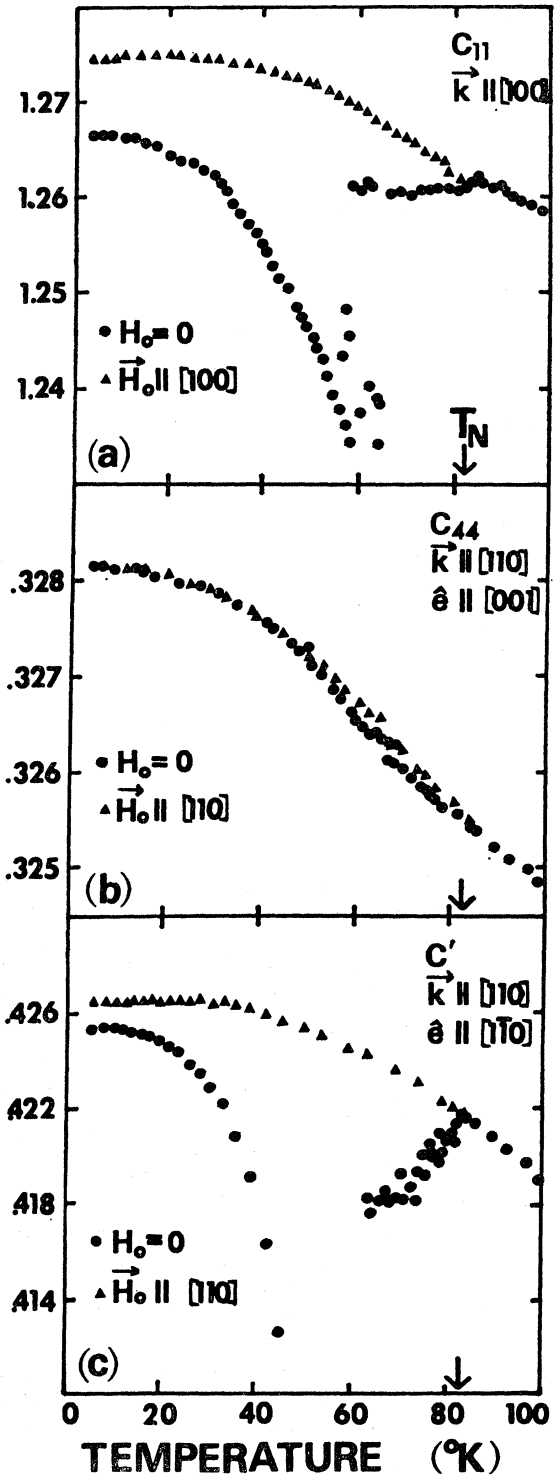

FIG. 6. Elastic constants C_{11}, C_{44}, and C' of $RbMnF_3$ versus temperature in the antiferromagnetic state. The vertical scale is in units of 10^{12} erg/cm^3.

IV. DISCUSSION OF RESULTS

The discussion of three somewhat overlapping temperature regions will be given separately.

A. Paramagnetic Region

For all temperatures $T>T_N$ the adiabatic elastic constants were independent of magnetic field to within $\pm 0.002\%$. Over the temperature range 180–300°K, the variation with temperature of each of the elastic constants is quite well described by a straight line of negative slope. Such behavior can be quite generally predicted from the thermodynamic theory of crystal lattices for temperatures $T>\Theta_D$. The free energy of the lattice may be written[35]

$$F=\varphi(V,e_{ij})+F_s(\omega_i,T)\,, \tag{4}$$

where $\varphi(V,e_{ij})$ is the static potential energy which is dependent only on the static coordinates of the nuclei (i.e., the strain e_{ij}) and the volume V of the sample, and $F_s(\omega_i,T)$ is the quantum-mechanical thermal free energy of the thermally excited lattice vibration modes of frequency ω_i. In the harmonic approximation ω_i is independent of e_{ij} and $\varphi(V,e_{ij})$ is independent of T. Thus the elastic constants are temperature-independent. Anharmonic forces can be included by retaining higher than quadratic terms in e_{ij} in $\varphi(V,e_{ij})$ and by making ω_i strain-dependent. On taking the appropriate second derivatives with respect to strain to obtain the elastic constant, the contribution from $F_s(\omega_i(e_{ij}),T)$ is found to be proportional to $E(T)$, the average vibrational energy per mode which has the value kT at high temperatures and $\frac{1}{2}\hbar\omega$ at low temperatures. The effect of the thermal term F_s is eliminated by the extrapolation procedure described in Sec. III. In $RbMnF_3$ the linear behavior of C_{ij} with temperature appears to extend down to $T\simeq\frac{1}{2}\Theta_D$.

As expected, the athermal values of C_{11} and $C'=\frac{1}{2}(C_{11}-C_{12})$ are larger than the measured values at low temperatures due to anharmonic effects associated with the zero point motion. However, C_{44} has the opposite behavior, the athermal value being slightly less than the measured low-temperature value. This anomalous result is not understood at the present time. The experimental situation is the same regardless of whether C_{44} is measured by propagation of transverse waves along the [100] axis or the [110] axis. It is possible, but seems unlikely, that the true high-temperature linear behavior has not been reached at 300°K and that higher-temperature measurements would show linear behavior with a sharper slope. In the temperature range $75<T<130$°K the $C_{44}(T)$ curve shows a slight concavity upward (Fig. 4) which is not observed in the behavior of the other elastic constants (Figs. 2, 3, and 5).

The pure elastic value of C_{12} as calculated from C_{11} and C' or from C_{11}, C_L, and C_{44} remains essentially constant over the entire range of temperature $4.2<T<300$°K with the value of $0.422\pm 0.004\times 10^{12}$ erg/cm^3 (note that 1 erg/cm^3=1 dyn/cm^2), except for a small decrease just discernible in the scatter near $T=T_N$. In zero magnetic field, some uncertainty exists in the

neighborhood of 60°K, but there appears to be a 1–2% peak in this region. The Cauchy ratio C_{44}/C_{12} decreases monotonically from 0.778±0.008 at 4.2°K to 0.755 ±0.008 at 300°K, its temperature dependence being almost entirely due to that of C_{44}. The anisotropy ratio $A=2C_{44}/(C_{11}-C_{12})$ increases monotonically from its value of 0.7695±0.002 at 4.2°K to a value of 0.8490 ±0.002 at 300°K. In zero magnetic field the anisotropy ratio shows an anomalous peak at $T\simeq 60$°K; it varies quite linearly with temperature for $180<T<300$°K.

In their treatment of the lattice dynamics of crystals with the cubic perovskite structure, Rajagopal and Srinivasan[36] considered only nearest-neighbor forces and neglected Coulomb forces. By making simplifying assumptions the number of independent force constants was reduced from the 10 deduced from symmetry considerations to three. In terms of the elastic constants of $RbMnF_3$ at 300°K, these force constants are

$$\alpha=2aC_{44}=27.02\pm0.05\times10^3 \text{ dyn/cm},$$
$$\beta=a(3C_{44}-C_{11})=-9.15\pm0.1\times10^3 \text{ dyn/cm}, \quad (5)$$
$$\zeta=\tfrac{1}{2}a(C_{44}-C')=-1.21\pm0.02\times10^3 \text{ dyn/cm}.$$

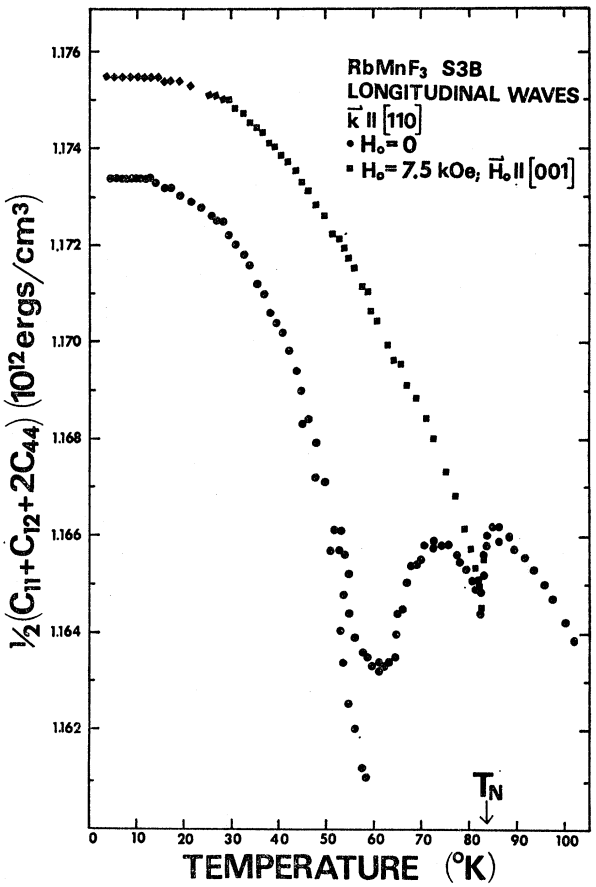

FIG. 7. Elastic constant C_L of $RbMnF_3$ (on expanded scale) versus temperature in the antiferromagnetic state.

[36] A. K. Rajagopal and R. Srinivasan, J. Phys. Chem. Solids 23, 633 (1962).

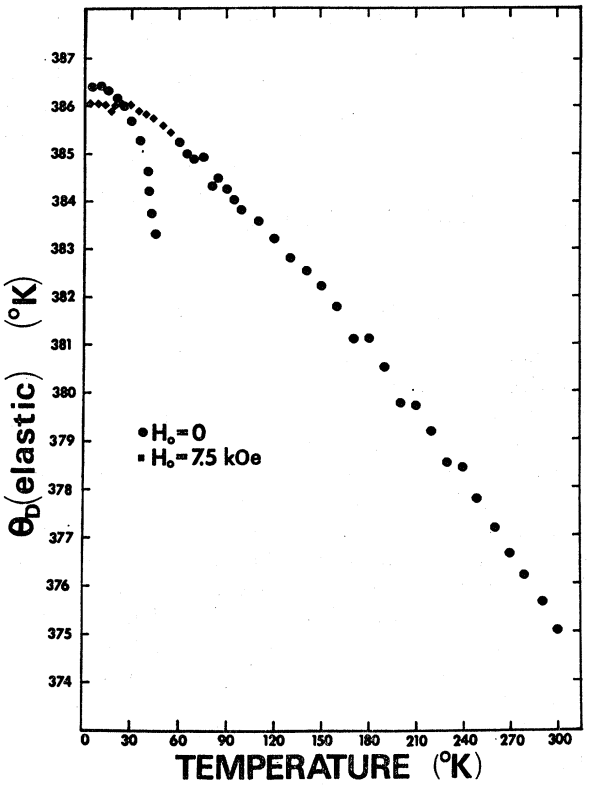

FIG. 8. Debye temperature Θ_D (elastic) as calculated from the elastic constants of Figs. 2–4 using Eq. (3).

When these values are used in the secular determinant to determine the long-wavelength optical mode frequencies,[36] one finds that one mode is unstable (i.e., has an imaginary frequency). Thus this three-constant model is not a satisfactory description of the lattice dynamics of $RbMnF_3$. Cowley[37] has presented a more comprehensive treatment of the lattice dynamics of the perovskite structure involving more than three parameters. Axe and Pettit[22] have given the experimental infrared reflectivity spectrum in several perovskite fluorides.

It is well established that in the limit of very low temperatures ($T\lesssim\Theta_D/50$)[34,38] the value of the Debye temperature Θ_D calculated from specific-heat measurements agrees, in most cases, with the value obtained from elastic-constant measurements. At higher temperatures the two values deviate from one another considerably because the specific heat is affected by the thermally excited high-frequency modes which show considerable deviation from the Debye density of states. On this basis one might expect that the value of Θ_D(elastic) would be independent of temperature since ultrasonic velocity measurements are typically made in the very-low-frequency end of the vibration spectrum.

[37] R. A. Cowley, Phys. Rev. 134, A981 (1964).
[38] T. H. K. Barron and M. L. Klein, Phys. Rev. 127, 1997 (1962).

However, the low-frequency modes interact anharmonically with the thermally excited high-frequency modes from the non-Debye part of the spectrum. These anharmonic interactions result in the $\sim 3\%$ decrease in the value of Θ_D(elastic) as the temperature is raised to 300°K as shown in Fig. 8. The magnetoelastic coupling (see Sec. IV C) results in the anomalously sharp decrease in Θ_D(elastic) with temperature for $T<60$°K and $H_0=0$.

B. Critical Region $T\simeq T_N$

Although no attempt has been made here to study quantitatively the critical behavior of the elastic properties of $RbMnF_3$ near T_N, several conclusions can be drawn from Figs. 6 and 7. For $T<T_N$ the *apparent* critical behavior is sharply magnetic-field-dependent. Care must be taken in interpreting critical behavior in this region to differentiate between true critical scattering effects and the magnetoelastic effects discussed in Sec. IV C. Thus we consider only the pure elastic constants in the following discussion. Examination of Figs. 6 and 7 (see also Refs. 8 and 10) reveals that the elastic constants obtained from longitudinal wave propagation (C_{11} and C_L) both show sharp minima at the Néel temperature T_N $(\Delta C_{11}/C_{11})\simeq 2.3\times 10^{-3}$ and $\Delta C_L/C_L\simeq 2.7\times 10^{-3}$. However, neither of the elastic constants derived from transverse wave propagation (C' and C_{44}) shows any effect of the magnetic ordering to within the accuracy of 2 parts in 10^5. Thus one can conclude that in $RbMnF_3$ if these transverse modes are coupled to the critical fluctuations near $T\simeq T_N$ at all, the coupling is some two orders of magnitude smaller than for the longitudinal modes. In a recent theoretical investigation of a Heisenberg paramagnet near the antiferromagnetic ordering temperature ($T\gtrsim T_N$), Pytte and Bennett[39] showed that the ultrasonic attenuation due to spin-phonon interactions has different effective coupling constants depending on the type of elastic mode being propagated and on the type of spin-phonon interaction considered, i.e., either volume magnetostriction or single-ion magnetostriction.[40] They find that for volume magnetostriction the effective coupling to the two longitudinal modes C_{11} and C_L is the same and the coupling to the C' and C_{44} transverse modes is zero. On the other hand, for the case of single-ion magnetostriction, although the coupling to the two longtudinal modes is of the same order of magnitude, the coupling to the two transverse modes C_{44} and $C'=\frac{1}{2}(C_{11}-C_{12})$ is not zero. In fact, the coupling to C' is predicted to be of the same order of magnitude as that for the longitudinal modes. Assuming that these same coupling coefficients would enter into the corresponding expressions for the change in the elastic constants derived from the four modes considered above, our experimental data (Figs. 6 and 7) are consistent only with the conclusion that the critical scattering of ultrasonic waves in $RbMnF_3$ is a result of the volume magnetostriction interaction and not the single-ion magnetostriction.

Neighbours and Moss[41] have independently reached the conclusion that the volume magnetostriction is the dominant interaction causing the increase in the ultrasonic attenuation in MnF_2 near the Néel temperature.

C. Antiferromagnetic Region—Magnetoelastic Coupling

The phenomenological form of the magnetoelastic interaction[42] in a two sublattice model of a cubic antiferromagnet is written[24]

$$E_{ME}=\frac{B_1}{M_0^2}\sum_{\substack{i=1,2\\ j=x,y,z}} M_{ij}^2 e_{jj}+\frac{B_3}{M_0^2}\sum_{j=x,y,z} M_{1j}M_{2j}e_{jj}$$
$$+\frac{B_2}{M_0^2}\sum_{i=1,2}(M_{ix}M_{iy}e_{xy}+\text{c.p.})$$
$$+(B_4/M_0^2)[(M_{1x}M_{2y}+M_{1y}M_{2x})e_{xy}+\text{c.p.}], \quad (6)$$

where the B_k, $k=1, 2, 3, 4$ are the coupling constants, only two of which are independent, M_{ij} is the jth ($j=x, y, z$) component of the ith ($i=1, 2$) sublattice magnetization, M_0 is the saturation value of the sublattice magnetization, and e_{ij} are the strains defined by

$$e_{ij}=(1-\tfrac{1}{2}\delta_{ij})(\partial u_i/\partial x_j+\partial u_j/\partial x_i). \quad (7)$$

c.p. denotes cyclic permutation. The interaction (6) serves to couple the dispersionless pure elastic modes of the system to the antiferromagnetic resonance modes. The solution (as shown in II) to the coupled equations of motion in the weak-coupling limit for the case of quasielastic longitudinal waves propagating along the [001] axis is given in the form of an effective elastic constant C_{11}^*:

$$C_{11}^*=C_{11}-4b_1\cos^2\theta+4\frac{\gamma\omega_E}{M_0}b_1^2\frac{\sin^2 2\theta}{\omega_+^2}$$
$$\times\left(1-\frac{3K}{b_1}[1-\tfrac{3}{2}\sin^2\theta]-\frac{H_0}{4H_E}\frac{H_0M_0}{b_1}\frac{\sin 2\varphi}{\sin 2\theta}\right). \quad (8)$$

In the derivation of this expression we have assumed frequencies much less than the Mn^{55} nuclear Larmor

[39] E. Pytte and H. S. Bennett, Phys. Rev. **164**, 712 (1967).

[40] See Table I of Ref. 39. Note that for $RbMnF_3$, $G_{11}\simeq 5G_{44}$ (Ref. 24). The effective coupling constant for single-ion magnetostriction for C_{11}, C_L, and C' is $\sim G_{11}^2$ while for C_{44} it is G_{44}^2. The conclusion drawn in the text that the volume magnetostriction is dominant is based primarily on the facts that C' and C_{44} show no anomaly near T_N [Figs. 6(b) and 6(c)] and that

$$\Delta C_{11}/C_{11}\simeq\Delta C_L/C_L.$$

[41] J. R. Neighbours and R. W. Moss, Phys. Rev. **173**, 542 (1968).

[42] We consider here both single-ion magnetostriction and dipolar magnetostriction, but exclude volume magnetostriction.

frequency ($\sim$680 MHz) at 4.2°K. C_{11} is the pure elastic constant, $b_1=B_1-\frac{1}{2}B_3$, and the other symbols are as defined by Cole and Ince.[26] Using the fact that $b_1 \ll K$ (anisotropy constant) for $RbMnF_3$ and considering the case of $\mathbf{H}_0 \| \mathbf{k} \| [001]$, Eq. (8) reduces to

$$C_{11}^* = \begin{cases} C_{11}-\frac{4}{3}b_1^2/K: & H_0 \leq (\frac{3}{2}H_E H_A)^{1/2} \\ C_{11} \quad\quad\quad : & H_0 \geq (\frac{3}{2}H_E H_A)^{1/2}. \end{cases} \tag{9}$$

On increasing the magnetic field through the value $(\frac{3}{2}H_E H_A)^{1/2}$, Eq. (9) predicts an increase in the measured value of the elastic constant C_{11}^* by the amount $4b_1^2/3K$. This is the observed behavior (Figs. 2 and 6). Since for $H_0 > (\frac{3}{2}H_E H_A)^{1/2}$, $C_{11}^* = C_{11}$, we are justified in denoting the upper data points in Figs. 2 (solid squares) and 6 (solid triangles) as the pure elastic constants; the lower curves represent the effective elastic constants ($C_{11}^* \neq C_{11}$).

The physical process which causes this rather large difference between the effective and pure elastic constants is in some ways unique. In the low-frequency limit the change $C_{11}^* - C_{11}$ is frequency-independent and does not result from tuning the antiferromagnetic resonance modes with the magnetic field to the ultrasonic frequency as is the case in most ultrasonic experiments in ferrimagnets.[43] In the present situation, the change in C_{11}^* is due to the fact that as H_0 is increased, the static equilibrium orientation of the sublattice magnetizations changes[26] with respect to $\mathbf{H}_0$ and $\mathbf{k}$, thus causing the effective coupling constant between the ultrasonic wave and the antiferromagnetic resonance modes to be magnetic-field-dependent.

The temperature dependence of $C_{11}^* - C_{11}$ is given by the ratio

$$b_1^2(T)/K(T).$$

The experimental values of $b_1(T)$ and $K(T)$ in $RbMnF_3$ have been measured, respectively, by Eastman[24] and by Freiser *et al.*[25] The qualitative behavior of the ratio $b_1^2(T)/K(T)$ is to increase from zero at $T=T_N$ to a maximum a few degrees below T_N and slowly decrease to its limiting low-temperature value. $C_{11}^* - C_{11}$ shows this type of behavior as seen from the data of Figs. 2 and 6(a). In the region of the maximum in $b_1^2(T)/K(T)$, the experimental behavior shows that the weak-coupling limit in which Eq. (8) was derived is no longer valid. As discussed in Secs. II and III, the strong magnetoelastic coupling in this region ($T \simeq 60$°K) manifests itself as structure on the cw mechanical resonances and a nonexponentially decaying pulse-echo pattern.

The model of magnetoelastic coupling outlined here will be discussed in some detail and quantitatively compared with experiment in II.

[43] R. C. LeCraw and R. L. Comstock, *Physical Acoustics*, edited by W. P. Mason (Academic Press Inc., New York, 1965), Vol. III B.

V. CONCLUSIONS

The elastic properties of $RbMnF_3$ have been measured over the temperature range 4.2–300°K using a cw transmission technique. The values of the elastic constants at 300°K do not agree with those reported previously by Eastman.[24] In the paramagnetic region ($T > T_N = 83$°K) the elastic constants C_{11}, C_{33}, and C' all decrease smoothly with increasing temperature, the decrease being quite linear for $T > \frac{1}{2}\Theta_D$. The constant C_{12} is independent of temperature in this region. The athermal values of C_{11} and C' are greater than the measured low-temperature values, but for C_{44} the measured value is higher. A three-force-constant model of the cubic perovskite structure was found to be not applicable to $RbMnF_3$.

Only the longitudinal elastic modes show the effect of critical scattering for $T \simeq T_N$. To within the experimental accuracy, C_{44} and C' are not affected by the onset of long-range order. This is consistent with the theory of Pytte and Bennett if the dominant spin-phonon interaction is taken to be the volume magnetostriction.

The very strong magnetic-field dependence of the effective elastic constants in the antiferromagnetically ordered state of $RbMnF_3$ is a result of the dependence of the equilibrium orientation of the magnetic sublattices on the magnitude and orientation of applied magnetic fields. In a forthcoming paper (II) the theory of magnetoelastic effects in $RbMnF_3$ will be presented and a quantitative comparison to experiment will be made.

ACKNOWLEDGMENTS

The authors are indebted to Dr. R. W. H. Stevenson for making available the single-crystal specimens used in this study. The chemical analysis was performed by the Analytical Chemistry Facility of the Materials Science Center at Cornell University under the direction of Dr. R. Skogerboe.

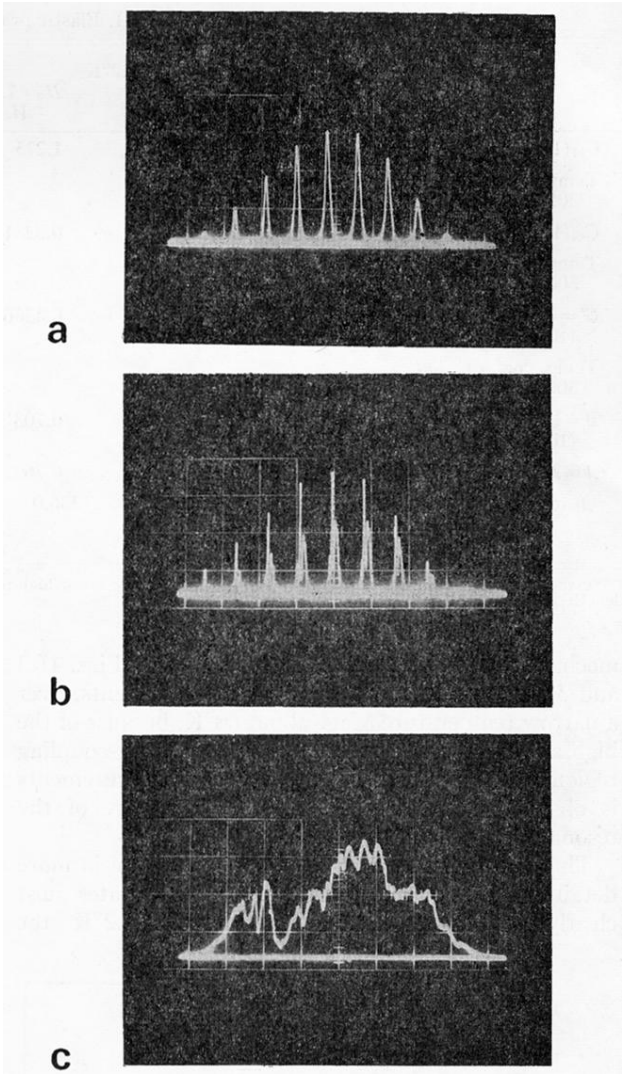

FIG. 1. Mechanical response patterns for 30 MHz ultrasonic waves in $RbMnF_3$ No. *S3B*, $H_0=0$. (a) longitudinal waves, $\mathbf{k}\|[110]$, $T=77.4°K$; (b) longitudinal waves, $\mathbf{k}\|[110]$, $T=54.6°K$; and (c) transverse waves, $\mathbf{k}\|[110]$, $\delta\|[1\bar{1}0]$, $T=77.4°K$. Receiver gain increased in (c) by 28 dB over that in (a) and (b).